Photoabsorption spectra of silver in the 4*d*-subshell excitation region

M. Aslam Baig*
Atomic and Molecular Physics Laboratory, Department of Physics, Quaid-i-Azam University, 45320 Islamabad, Pakistan and Physikalishec Institute der Universitat Bonn, Nussallee-12, Bonn, Germany
(Received 27 November 2008; published 22 January 2009)

High-resolution measurements of the photoabsorption spectra of silver in the 4*d*-subshell excitation region are reported using synchrotron radiation as the background source of the continuum. The spectra were recorded in the first order of a 3-m spectrograph equipped with a 6000-lines/mm holographic grating at a dispersion of 0.5 nm/mm and using photographic detection. Rydberg series have been observed converging to four conspicuous limits built on the $4d^9 5s$ parent ion configuration $4d^{10}5s\ ^2S_{1/2} \rightarrow 4d^9 5s(^3D_{3,2,1}, ^1D_2)\ np$ and nf ($J=1$). The high-resolution data reveal extended Rydberg series, accurate term energies, quantum defects, and widths of the autoionizing resonances. The resonance energies and widths of the leading members of the series have been determined using multichannel quantum defect theory.

DOI: 10.1103/PhysRevA.79.012509 PACS number(s): 32.30.−r, 32.80.Aa, 32.80.Ee, 32.80.Zb

I. INTRODUCTION

The outermost *d*-subshell excitations in copper, silver, and gold yield much simpler sub-valence excitation spectra than the alkali-metal atoms since the $d \rightarrow p$ excitation dominates in intensity over the $d \rightarrow f$ excitation below the *d* thresholds, owing to strong centrifugal barrier effects. Since the resulting spectra lie above the first ionization threshold, therefore, autoionizing resonances are expected as a result of configuration interactions between discrete and continuum channels. Tegeder and Linck [1] measured the relative photoionization cross section of silver in the 160.0–120.0 nm wavelength region using an atomic beam technique. Subsequently, Johnsen and Linck [2] analyzed the terms arising from the $4d^9 5s5d$ configuration by comparison with arc spectra. The absorption spectrum of silver in the vacuum ultraviolet region was reported by Connerade *et al.* [3] who listed more than 50 previously unknown transitions attributed to 4*d*-subshell excitation and attempted a detailed analysis based on the *ab initio* Hartree-Fock calculations. Connerade and Baig [4] reinvestigated the 4*d*-subshell excitation spectra at a lower dispersion with the aim of recording the level structure of the $4d^9 5s5p$ configuration. This region was concurrently studied by Cantu *et al.* [5] using the flash pyrolysis technique. The ejected electron spectrum of silver was studied by James *et al.* [6], whereas Müller *et al.* [7] studied the autoionizing resonances belonging to the $4d^9 5s5p$ configuration using photoionization technique. Baier *et al.* [8] studied the autoionizing levels using a silver discharge and a laser excitation technique. The level structure of the $3d^9 4s6p$ and $3d^9 4s4f$ configurations in copper and the $4d^9 5s7p$ and $4d^9 5s4f$ configurations in silver were analyzed by Baig *et al.* [9] who presented a consistent level assignments for these atoms. Loock *et al.* [10] observed the highly excited $ns\ ^2S_{1/2}$ and $nd\ ^2D_{3/2,5/3}$ Rydberg levels using a two-color resonant excitation on a laser-vaporized atomic silver beam. Recently, Badr *et al.* [11] reported the frequency measurements, isotope shift, and hyperfine structure of the $4d^9 5s^2\ ^2D_{5/2} \rightarrow 4d^{10}6p\ ^2P_{3/2}$ transition in atomic silver. More recently, Pickering and Zilio [12] reported accurate energy levels of silver using Fourier transform spectrometry covering the wavelength region 200–828 nm.

The motivation behind the present work was to contribute to our ongoing project on high-resolution studies of the *d*-subshell excitation spectra of atoms: zinc, palladium, thallium, ytterbium, cadmium, copper, and mercury [13–19]. In this paper, we present the spectra of silver recorded at a much higher dispersion and resolution than the previously reported spectra. A full multiplicity of the level structure based on the $4d^9 5s\ np$ and nf configurations has been resolved and accurate term energies and quantum defects for each level have been determined.

II. EXPERIMENTAL DETAILS

The absorption spectrum of silver was photographed in the first order of a 3-m off-plane vacuum spectrograph equipped with a 6000-lines/mm holographic grating. Synchrotron radiation emitted by the 2.5-GeV electron accelerator at the Physikalisches Institute der Universitat Bonn, Germany served as a background source of continuum. Spectroscopically pure silver was evaporated in an induction furnace using a windowless vapor containment system. The furnace tubes were made of tantalum, 40 cm long, 15 mm outer diameter, and 0.2 mm wall thickness. About 3 g of silver wire was loaded in a tantalum boat, which was sufficient for several hours of experimentation. The temperature of the furnace was varied from 1400 to 1600 K depending on the vapor pressure required to observe the higher members of the Rydberg series. The spectra were photographed on the Kodak SWR plates with an exposure time between 2 and 6 min. The wavelength calibration under an identical illumination of the grating was achieved using the absorption spectra of molecular hydrogen [20,21] and krypton [22], which possess many sharp lines covering this spectral region. The plates were measured using an Abe-Comparator with an absolute accuracy of ± 0.003 nm. We used a third-order

*FAX: +92 51 9219888. baig@qau.edu.pk, baig77@gmail.com

Tchebichev Polynomial fit with an internal consistency of ± 0.002 nm to calculate the wavelengths of the unknown lines. The spectra recorded on the photographic plates were digitized with a computer-controlled microdensitometer. The transmission of the photographic plates was measured in steps of 5 μm using a slit width of 10 μm at the photomultiplier.

III. RESULTS AND DISCUSSION

The ground-state configuration of silver is $4d^{10}5s\ ^2S_{1/2}$. Excitation of the outer most $5s$ electron yields $5snp\ ^2P_{1/2,3/2}$ Rydberg series converging to the first ionization threshold. Brown and Ginter [23] observed these series up to $n=71$ and determined the first ionization potential of silver as 61 106.56(06) cm^{-1}. Ishikawa [24] reported the value 61 104.30(6) cm^{-1}, which was about 2.20 cm^{-1} lower than that listed in the NBS tables [25]. Recently, Loock *et al.* [10] reported this value as 61 106.45(20) cm^{-1}. The value determined by Brown and Ginter [23] is more accurate and therefore has been used in the data analysis.

The $4d$-subshell excitation spectrum of silver can be described by the following excitation scheme:

$$4d^{10}5s \rightarrow 4d^9 5snp \quad (n \geqslant 5)$$
$$nf \quad (n \geqslant 4).$$

From the $4d^{10}5s\ ^2S_{1/2}$ ground state, all the states with $J=1/2$ and $J=3/2$ are accessible in a photoabsorption experiment. In LS coupling the number of allowed transition is restricted to 4: two series to $4d^9 5s\ (^3D)$ and two series to the $4d^9 5s\ (^1D)$ ionic level. However, the observed spectra show numerous Rydberg series which converge to four limits. Therefore, in order to explain the observed structure we have adopted the j_cK-coupling scheme [26,27] for level designation. In this coupling scheme, the orbital angular momentum of the core electrons is strongly coupled, forming the j_c quantum number for the core electrons. The angular momentum of the core electrons ($j_c=3$, 2, 1, and 2) is then coupled to the orbital angular momentum of the excited electron to form the K quantum number, which is then weakly coupled to the spin quantum number of the excited electron to furnish the resultant J quantum number and the levels are designated as $n\ell\ [K]_J$. The expected Rydberg series converging to the four limits are

$$\begin{aligned} 4d^{10}5s\ ^2S_{1/2} \rightarrow\ & 4d^9 5s(^3D_3)np[2]_{1/2}, \\ & 4d^9 5s(^3D_2)np[1]_{1/2,3/2},[2]_{3/2}, \\ & 4d^9 5s(^3D_1)np[0]_{1/2},[1]_{1/2,3/2},[2]_{3/2}, \\ & 4d^9 5s(^1D_2)np[1]_{1/2,3/2},[2]_{3/2}. \end{aligned}$$

The level designation in j_cK coupling is more appropriate because of the large spin-orbit splitting of the parent ion levels. Keeping in view the degeneracy of the J components, the expected series are as follows: one np series to the $(^3D_3)$ limit at 100 270.46 cm^{-1}, two series to the $(^3D_2)$ limit at 101 847.56 cm^{-1}, three series to the $(^3D_1)$ limit at 104 845.26 cm^{-1}, and two series to the $(^1D_2)$ limit at 107 152.26 cm^{-1}. Due to the high resolution and dispersion experimental technique employed in the present work, the J components have also been resolved for the few leading members of the series. Since the fine-structure splitting decreases rapidly with increasing principal quantum number, therefore, at higher n values only the K components have been observed. Similarly the nf series built on the ionic levels are

$$\begin{aligned} 4d^{10}5s\ ^2S_{1/2} \rightarrow\ & 4d^9 5s(^3D_3)nf[0]_{1/2},[1]_{1/2,3/2},[2]_{3/2}, \\ & 4d^9 5s(^3D_2)nf[1]_{1/2,3/2},[2]_{3/2}, \\ & 4d^9 5s(^3D_1)nf[2]_{3/2}, \\ & 4d^9 5s(^1D_2)nf[1]_{1/2,3/2},[2]_{3/2}. \end{aligned}$$

Three series to the $(^3D_3)$ limit, two series to the $(^3D_2)$ limit, one series to the $(^3D_1)$ limit, and two series to the $(^1D_2)$ limit are expected. The identification of the spectral lines was made based on the analysis of the effective quantum numbers, line intensities, and line profiles of the series members. The converging limits of the observed series are calculated by adding the energies of the $4d^9 5s$ configuration based ionic levels to the first ionization potential of silver [23]. The quantum defects "μ" are then calculated using the Rydberg expression

$$E_n = \mathcal{V} - \frac{\mathcal{R}}{(n-\mu_\ell)^2},$$

where E_n is the energy of the nth level; $\mathcal{V}$ is the ionization potential; $\mathcal{R}$ is the mass-corrected Rydberg constant for silver, 109 736.758 cm^{-1}; n is the principal quantum number; and μ_ℓ is the quantum defect. Our general procedure for the level assignments was to identify the first few members of each series based on the regular change of the line spacing, consistent line shapes, and then to extend the series toward the higher n values. In some cases the series were extended from the higher n values to the leading members, keeping in view their quantum defects. Almost every line has been interpreted as belonging to Rydberg series converging to four limits built on the $4d^9 5s\ (^3D_{3,2,1}, {}^1D_2)$ parent ion levels. Connerade and Baig [4] and Müller *et al.* [7] studied the photoionization spectra of silver covering the $4d^9 5s6p$ configuration and all the expected levels of this configuration were observed. The level assignments suggested by Connerade and Baig [4] were confirmed by Heinzmann *et al.* [28] via spin polarization studies of these level. The *ab initio* Hartree-Fock calculations [3] for the $4d^9 5s6p$ configuration suggest that one must treat the levels belonging to $5s6p\ (^1P_1)4d^9$ and $5s6p\ (^3P_1)4d^9$ independently, because the Slater integrals are different for these configurations. The theoretical calculations were in good agreement with the relative intensities of the observed spectrum. It was also inferred that the LS designation is appropriate for the $4d^9 5s6p$ configuration and there is a smooth transition from LS to jj coupling with an increase of the principal quantum number.

In Fig. 1, the spectrum covering the region between 107.50 and 104.25 nm is produced which shows the lines belonging to the $4d^9 5s(^3D_{3,2})7p$ and $4d^9 5s(^3D_{3,2})4f$ configurations along with the $4d^9 5s(^3D_3)8p$ and $4d^9 5s(^3D_3)5f$ configurations at the lower-wavelength side. According to the

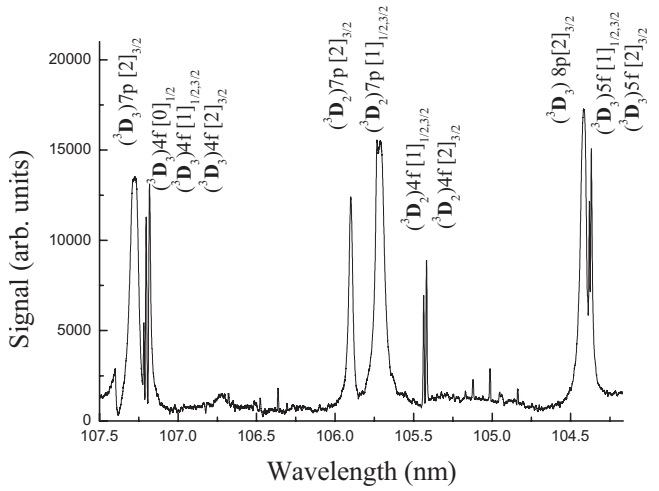

FIG. 1. Densitometer trace of the absorption spectrogram of silver in the 107.80–105.75-nm region showing the leading members of the series built on the $4d^9\ 5s\ (^3D_{3,2})$ ionic levels. The full multiplicity of the components has been resolved.

j_cK-coupling scheme level designation, only one np and three nf levels are expected attached to the $4d^95s(^3D_3)$ limit, and indeed we have observed all the K components for these levels. For the $4d^95s\ (^3D_2)$ limit, three $np\ [2]_{1/2}$, $[1]_{1/2}$, $[1]_{3/2}$ and two $nf\ [1]_{1/2,3/2}$ and $[2]_{3/2}$ lines are expected. The multiplet structure in the center of the figure around 105 nm corresponds to the $(^3D_2)7p\ [2]_{3/2}$, $[1]_{1/2,3/2}$ and $(^3D_2)4f\ [1]_{1/2,3/2}$, $[2]_{3/2}$ lines, respectively. The observed lines around 104 nm are the next member of the series built on the $4d^95s\ (^3D_3)$ limit: namely $8p\ [2]_{3/2}$ and $5f\ [0]_{1/2}$, $[1]_{1/2,3/2}$, $[2]_{3/2}$, respectively. The recorded spectrum provides a text book example of the j_cK-coupling-scheme-based level structure.

In Fig. 2 the spectrum covering the wavelength region between 103.25 and 101.00 nm is reproduced. The dominant lines in this region belong to the $(^3D_3)\ np\ [2]_{3/2}$ series

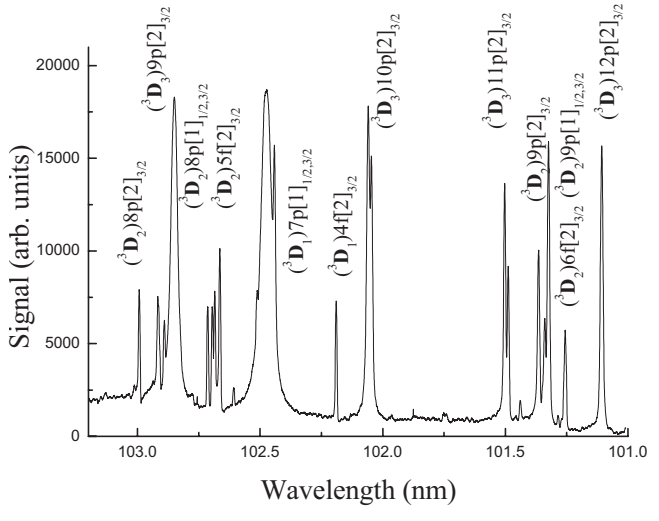

FIG. 2. Densitometer trace of the absorption spectrogram of silver in the 103.25–101.00-nm region showing the $4d^9\ 5s\ (^3D_3)$ $np\ (9 \leqslant n \leqslant 12)$ and $4d^9\ 5s\ (^3D_2)\ np\ (8 \leqslant n \leqslant 9)$ series in addition to the fully resolved levels of the $4d^9\ 5s\ (^3D_1)\ 7p$ and $4f$ configurations around 102.5 nm.

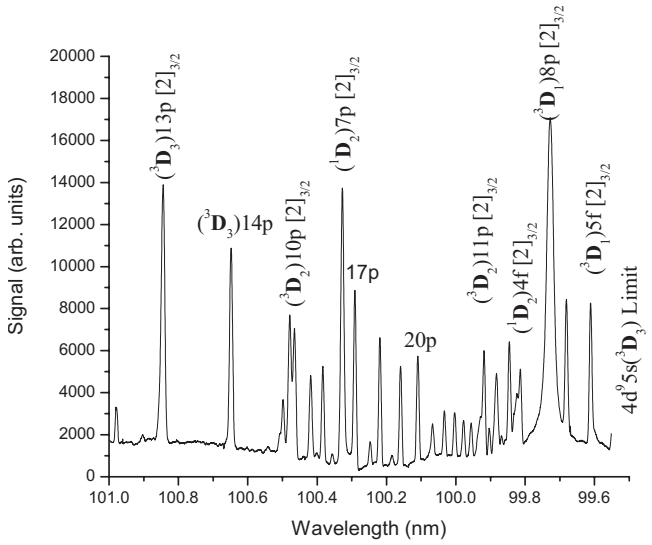

FIG. 3. Densitometer trace of the absorption spectrogram of silver in the 101.00–98.65-nm region showing the $4d^9\ 5s\ (^3D_3)\ np$ Rydberg series $(13 \leqslant n \leqslant \text{limit})$. The leading members of the series attached to the $4d^9\ 5s\ (^1D_2)$ limit $7p$ around 100.3 nm and $4f$ around 99.8 nm are also evident.

$(9 \leqslant n \leqslant 12)$ besides the leading members of the series built on the $4d^95s(^3D_1)$ level and two members of the series ($n = 8$ and 9) built on the $4d^95s(^3D_2)$ level. The lines observed around 102 nm are assigned as $(^3D_1)7p\ [0]_{1/2}$, $[2]_{3/2}$, $[1]_{3/2,1/2}$ and $(^3D_1)\ 4f\ [2]_{3/2}$, respectively. The two sharp lines in between the $(^3D_1)7p\ [0]_{1/2}$ and $[2]_{3/2}$ lines are identified as $(^3D_2)5f\ [1]_{1/2,3/2}$ and $[2]_{3/2}$. All the other observed lines in this region have also been given appropriate assignment.

The absorption spectrum of silver covering the spectral region from 101.0 nm to 99.5 nm is reproduced in Fig. 3 showing the higher members of the $np\ [2]_{3/2}$ Rydberg series $(13 \leqslant n \leqslant \text{limit})$ attached to the $4d^95s\ (^3D_3)$ level. The dominant line in this spectrum, at the lower-wavelength region, is identified as $(^3D_1)8p\ [2]_{3/2}$ and the nearby lines as $(^3D_1)8p\ [1]_{1/2,3/2}$ and $(^3D_1)5f\ [2]_{3/2}$. The presence of these lines near the $(^3D_3)$ series limit hampers the detection of the higher member of the series attached to this limit. In this region, the leading members of the series attached to the $4d^95s\ (^1D_2)$ limit are also apparent, $4d^95s\ (^1D_2)7p[2]_{3/2}$ at 100.35 nm and $(^1D_2)\ 4f\ [2]_{3/2}$ at 99.82 nm. Interestingly, the widths of these lines are comparable to that of the adjacent members of the Rydberg series, apparently the broadening due to autoionization is scarce. Besides, in the vicinity of these lines the intensities of the $(^3D_3)\ np\ [2]_{3/2}$ Rydberg series are altered. Largely the np lines possessing $J=3/2$ are broad, whereas the nf lines remain very sharp except the leading member of the $(^3D_3)\ nf\ [2]_{3/2}$ series. The broadening of the np lines is attributed to the autoionization phenomena, which can be described as mixing of the $4d^95snp_J$ quasidiscrete states with the $4d^{10}\ \varepsilon p\ J=1/2,\ 3/2$ continuum states. According to the autoionization selection rules, only the p states can be mixed by the electrostatic interaction $(\frac{e^2}{r_{ij}})$ of the electrons. Therefore, the strengths and the widths of the autoionizing lines reflect the ^2P composition in the wave functions of the per-

tinent levels through the matrix elements of the electric-dipole transitions $\langle 4d^9 5snp\ ^2P_J|D|4d^{10}5s\ ^2S_{1/2}\rangle$ and the mixing of the quasidiscrete states with the continuum states $\langle 4d^{10}\varepsilon pP_J|V|4d^9 5snpP_J\rangle$, respectively. The $4d^9 5snf$ levels do not interact with the available continuum due to the nonavailability of the nf continuum states, and consequently the lines remain relatively sharp. However, some lines do show Fano-type line shapes, which is attributed to the parity-allowed autoionization.

In order to extract the multichannel quantum defect theory (MQDT) parameters from the observed line shapes of the autoionizing resonances, we have used the formalism as described by Cooke and Cromer [29], Giusti-Suzor and Fano [30], Ueda [31], and Gallagher [32]. A generalized expression to represent the photoionization cross section with one open and $n-1$ bound channels has been derived by Baig and Bhatti [33] as

$$\sigma = K \frac{\left| \sum_{1}^{n} C_{1i}^2 D_i \right|^2}{C_{11}^2 + \left| \sum_{2}^{n} C_{1i}^2 R_{1i} \right|^2}. \tag{1}$$

Here K is a constant, C_{1i} are the cofactors of the first row of the MQDT matrix, and D_i are the transition dipole moments between the initial state and the ith channel. The summation in the numerator is over all the n channels involved, while in the denominator the summation is only over the $n-1$ bound channels. We consider here the lowest autoionizing lines attached to the $4d^9 5s\ ^3D_{3,2,1}$ and $^1D_2$ limits. The $4d^{10}(^1S_0)\ \varepsilon p$ channel is considered as the generalized continuum in which the $4d^9 5sn\ell$ Rydberg sates mainly decay. In Fig. 4, we show a densitometric trace of the absorption spectrum in the 93 000–93 500 cm^{-1} region showing the line shapes of the $(^3D_3)7p\ [2]_{3/2}$ and $(^3D_3)\ 4f\ [0]_{1/2}$, $[1]_{1/2,3/2}$, and $[2]_{3/2}$ autoionizing resonances. The $(^3D_3)7p\ [2]_{3/2}$ is the broadest line, and $(^3D_3)\ 4f\ [0]_{1/2}$, $[1]_{1/2,3/2}$, and $[2]_{3/2}$ remain relatively sharp, whereas, the line shape of $(^3D_3)4f\ [2]_{3/2}$ is asymmetric. The line profile of the $7p[2]_{3/2}$ resonance is

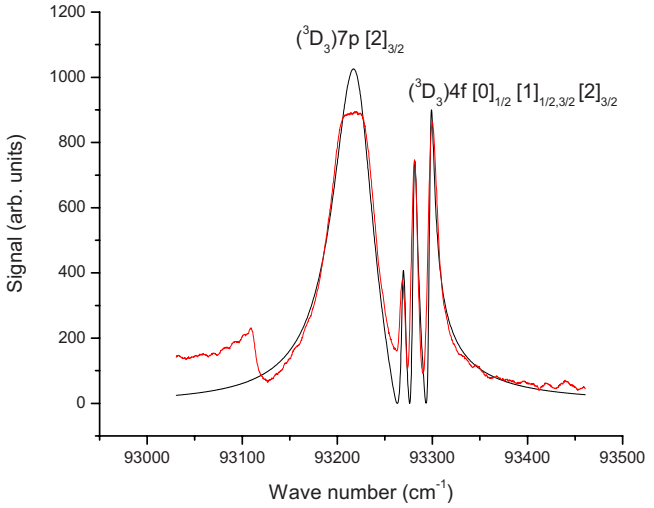

FIG. 4. (Color online) The line shapes of the autoionizing resonances $(^3D_3)7p[2]_{3/2}$ and $(^3D_3)4f[0]_{1/2}$, $[1]_{1/2,3/2}$, and $[2]_{3/2}$ along with the simulated spectrum using five-channel quantum defect theory. The experimentally observed profile of the $(^3D_3)7p[2]_{3/2}$ line is saturated at the peak position.

Lorentzian, which reveals that the transition dipole moment between the ground state and the continuum state is negligibly small. The asymmetric line shape is a reflection of different dipole moments to the bound and continuum channels and the different phase shifts of these channels relative to the ground state. This part of the spectrum is described as a five-channel MQDT problem with one open and four closed channels. Further, it is considered that the interactions among the bound channels are negligible. The next step is to extract the eigenquantum defects and the interaction parameters which are primarily responsible for the widths of the resonances. The five channels comprise of a generalized continuum as channel—1, $(^3D_3)\ np\ [2]_{3/2}$ channel—2, $nf\ [0]_{1/2}$ channel—3, $nf\ [1]_{1/2,3/2}$ channel—4, and $nf\ [2]_{3/2}$ channel—5. The five-channel quantum defect theory matrix is written as

$$\begin{pmatrix} \tan \pi(\nu_1+\delta_1) & R_{12} & R_{13} & R_{14} & R_{15} \\ R_{21} & \tan \pi(\nu_2+\delta_2) & R_{23} & R_{24} & R_{25} \\ R_{31} & R_{32} & \tan \pi(\nu_3+\delta_3) & R_{34} & R_{35} \\ R_{41} & R_{42} & R_{43} & \tan \pi(\nu_4+\delta_4) & R_{45} \\ R_{51} & R_{52} & R_{53} & R_{54} & \tan \pi(\nu_5+\delta_5) \end{pmatrix} = 0. \tag{2}$$

Here δ_i are the eigenquantum defects and R_{ij} are the interchannel interaction parameters. A comparison between the experimentally observed spectra and the simulated spectra using the following MQDT parameters is shown in Fig. 4:

$$\begin{aligned} &D_1 = -0.5, \quad D_2 = 4.8, \quad D_3 = 1.0, \quad D_4 = 1.5, \quad D_5 = 1.8, \\ &\delta_2 = 0.056, \quad \delta_3 = 0.041, \quad \delta_4 = 0.038, \quad \delta_5 = 0.032, \\ &R_{12} = 0.15, \quad R_{13} = 0.05, \quad R_{14} = 0.055, \quad R_{15} = 0.060. \end{aligned}$$

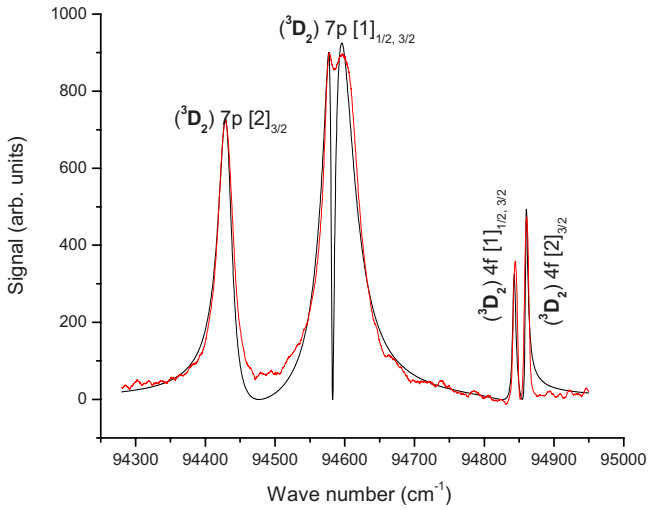

FIG. 5. (Color online) The line shapes of the autoionizing resonances $(^3D_2)7p[2]_{3/2}$ $[1]_{1/2,3/2}$ and $(^3D_2)4f[1]_{1/2,3/2}$ and $[2]_{3/2}$ along with the simulated spectrum using six-channel quantum defect theory.

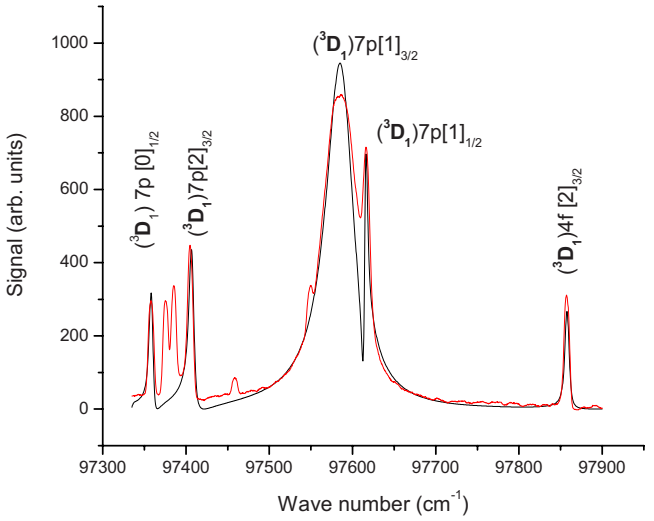

FIG. 6. (Color online) The line shapes of the autoionizing resonances $(^3D_1)7p[0]_{1/2}$, $[2]_{3/2}$, $[1]_{1/2,3/2}$ and $(^3D_1)4f[2]_{3/2}$ along with the simulated spectrum using six-channel quantum defect theory.

From these parameters the widths of the autoionizing resonances have been determined using the expression [29–32]

$$\Gamma(\mathrm{cm}^{-1}) = \frac{4R_{\mathrm{Ag}}R_{ij}^2}{\pi\nu_i^3}. \tag{3}$$

Here ν_i is the effective quantum number with respect to the $4d^9 5s$ $(^3D_3)$ ionization limit and R_{Ag} is the mass corrected Rydberg constant for silver. The MQDT parameters show that the interaction between the continuum channel and the $np[2]_{3/2}$ channel is nearly 3 times larger than that of the nf $[2]_{3/2}$ channel and about 3 times larger than the interaction between the continuum and the nf $[1]_{1/2,3/2}$ channel. The resonance width of $7p$ $[2]_{3/2}$ is determined as 50(10) cm^{-1} and that for $4f$ $[0]_{1/2}$, $[1]_{1/2,3/2}$, and $[2]_{3/2}$ as 6(1) cm^{-1}, 7(1) cm^{-1}, and 9(1) cm^{-1}, respectively.

The corresponding levels attached to the $4d^9 5s$ $(^3D_2)$ limit are reproduced in Fig. 5 covering spectral the region 94 200–94 950 cm^{-1}. The spectrum is represented by the six-channel MQDT formalism. We define the generalized continuum as channel—1, $(^3D_2)$ np $[2]_{3/2}$ as channel 2, $np[1]_{1/2,3/2}$ as channels 3 and 4, $nf[1]_{1/2,3/2}$ as channel 5, and $nf[2]_{3/2}$ as channel 6. The experimentally recorded spectra and the simulated spectra are shown in Fig. 5 are in excellent agreement. The following MQDT parameters have been used to simulate the spectra:

$$\begin{aligned} &D_1 = -0.5, \quad D_2 = 2.7, \quad D_3 = 2.4, \quad D_4 = 3.8, \quad D_5 = 0.9, \quad D_6 = 0.1, \\ &\delta_2 = 0.154, \quad \delta_3 = 0.115, \quad \delta_4 = 0.110, \quad \delta_5 = 0.042, \quad \delta_6 = 0.037, \\ &R_{12} = 0.10, \quad R_{13} = 0.08, \quad R_{14} = 0.125, \quad R_{15} = 0.05, \quad R_{16} = 0.045. \end{aligned}$$

The widths of the $(^3D_2)$ $7p$ $[2]_{3/2}$ and $7p$ $[1]_{1/2,3/2}$ resonances are determined as 25(5) cm^{-1}, 15(4) cm^{-1}, and 37(6) cm^{-1}, whereas those of $4f$ $[1]_{1/2,3/2}$ and $4f$ $[2]_{3/2}$ as 6(1) cm^{-1} and 5(1) cm^{-1}, respectively.

The line shapes of the lowest members of the series built on the $4d^9 5s$ $(^3D_1)$ limit are shown in Fig. 6 covering the spectral region 97 300–97 950 cm^{-1}. This part of the spectrum is also treated using the six-channel QDT formalism. Here channel 1 is the continuum channel, channel 2 is $(^3D_1)$ $np[0]_{3/2}$, channel 3 is $np[2]_{3/2}$, channels 4 and 5 are $np[1]_{3/2}$ and $np[1]_{1/2}$, and channel 6 is $nf[2]_{3/2}$. The following MQDT parameters have been used to simulate the spectra:

$$\begin{aligned} &D_1 = 1.5, \quad D_2 = 0.8, \quad D_3 = 1.1, \quad D_4 = 4.0, \quad D_5 = 1.0, \quad D_6 = -0.8, \\ &\delta_2 = 0.171, \quad \delta_3 = 0.159, \quad \delta_4 = 0.112, \quad \delta_5 = 0.104, \quad \delta_6 = 0.037, \\ &R_{12} = 0.04, \quad R_{13} = 0.05, \quad R_{14} = 0.13, \quad R_{15} = 0.03, \quad R_{16} = 0.045. \end{aligned}$$

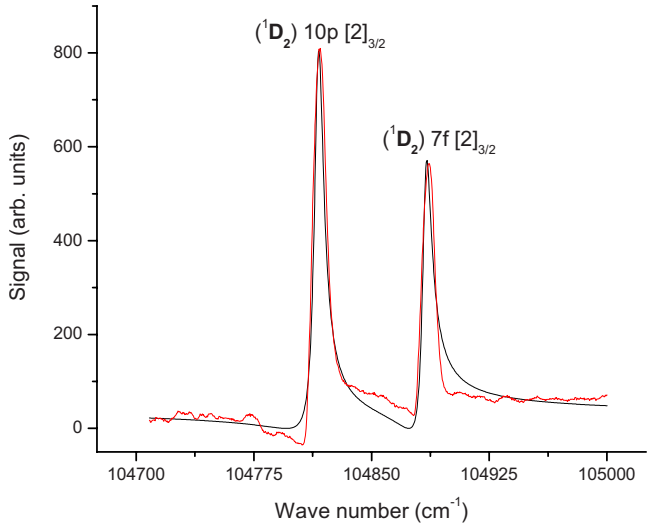

FIG. 7. (Color online) The line shapes of the autoionizing resonances $(^1D_2)10p[2]_{3/2}$ and $(^1D_2)4f[2]_{3/2}$ along with the simulated spectrum using three-channel quantum defect theory.

The widths of the $(^3D_1)7p$ $[0]_{1/2}$, $(^3D_1)7p$ $[2]_{3/2}$, $(^3D_1)7p$ $[1]_{3/2}$, and $7p$ $[1]_{1/2}$ resonances have been determined as 4(1) cm^{-1}, 6(1) cm^{-1}, 40(6) cm^{-1}, and 2(1) cm^{-1}, respectively, whereas that of the $4f$ $[2]_{3/2}$ resonance as 5(1) cm^{-1}.

As far the levels attached to the $4d^95s$ $(^1D_2)$ limit are concerned, we have located a single line corresponding to the $4d^95s$ $(^1D_2)7p$ configuration and also a single line for the $4d^95s(^1D_2)$ $4f$ configuration instead of at least two K components for each configuration. Furthermore, these lines remain sharp, apparently no broadening due to autoionization (see Fig. 3). The reason why the full multiplicity of the levels could not be resolved for the singlet-based configurations is not yet clear, and therefore more work is needed in this direction. The clearly resolved structures of the p and f resonances built on the $4d^95s$ $(^1D_2)$ limit that lie adjacent to the $4d^95s$ $(^3D_1)$ limit are shown in Fig. 7 covering the energy region 104 700–105 000 cm^{-1}. The lines are identified as $(^1D_2)$ $10p[2]_{3/2}$ and $7f$ $[2]_{3/2}$, respectively. The line profiles are asymmetric with a clear minimum in the cross section, evidence of the contribution of direct ionization to the available continuum. To simulate the observed spectra, we have used a three-channel model of the quantum defect theory where the cofactors are described as

$$C_{11} = (\varepsilon_2\varepsilon_3 - R_{23}^2), \quad C_{12} = -(\varepsilon_3 R_{12} - R_{13}R_{23}),$$
$$C_{13} = -(\varepsilon_2 R_{13} - R_{12}R_{23}). \tag{4}$$

Here ε_i $(i=1,2,3)$ represents $\tan[\pi(\nu_i+\delta_i)]$. Since both the autoionizing resonances are built on the same limit possessing the same J values, but with different L values, therefore, they are considered as noninteracting. Adjusting the parameter $R_{23}=0$ a simple analytical expression for photoionization cross section is written as

TABLE I. Level structure built on the $4d^95s$ $(^{1,3}D)7p$ and $4f$ configurations in silver.

Level assignments		λ (nm)	n^*	Γ (cm^{-1})
$4d^95s(^3D_3)7p$	$[2]_{3/2}$	107.277	3.944	50(10)
$4d^95s(^3D_3)4f$	$[0]_{1/2}$	107.217	3.959	6(1)
$4f$	$[1]_{1/2,3/2}$	107.202	3.962	7(1)
$4f$	$[2]_{3/2}$	107.180	3.968	9(3)
$4d^95s(^3D_2)7p$	$[2]_{3/2}$	105.878	3.846	25(5)
$7p$	$[1]_{1/2}$	105.712	3.885	15(5)
$7p$	$[1]_{3/2}$	105.691	3.890	37(8)
$4d^95s(^3D_2)4f$	$[1]_{1/2,3/2}$	105.415	3.958	6(1)
$4f$	$[2]_{3/2}$	105.397	3.963	5(1)
$4d^95s(^3D_1)7p$	$[0]_{1/2}$	102.699	3.829	4 (1)
$7p$	$[2]_{3/2}$	102.650	3.841	6 (1)
$7p$	$[1]_{3/2}$	102.458	3.888	40 (10)
$7p$	$[1]_{1/2}$	102.426	3.896	2 (1)
$4d^95s(^3D_1)4f$	$[2]_{3/2}$	102.175	3.963	5 (1)
$4d^95s(^1D_2)7p$	$[1]_{1/2,3/2}[2]_{3/2}$	100.325	3.831	7(1)
$4d^95s(^1D_2)4f$	$[1]_{1/2,3/2}[2]_{3/2}$	99.833	3.964	6(1)

$$\sigma = \frac{|\varepsilon_2\varepsilon_3 D_1 - \varepsilon_3 R_{12} D_2 - \varepsilon_2 R_{13} D_3|^2}{(\varepsilon_2\varepsilon_3)^2 + |\varepsilon_2 R_{13}^2 + \varepsilon_3 R_{12}^2|^2}. \tag{5}$$

The line profiles of these autoionizing resonances have been simulated using the following MQDT parameters:

$$D_1 = -6.0, \quad D_2 = 3.7, \quad D_3 = 3.0,$$
$$\delta_2 = 0.147, \quad \delta_3 = 0.044,$$
$$R_{12} = 0.13, \quad R_{13} = 0.13.$$

The experimental spectra along with the fitted line profiles are reproduced in Fig. 7. The widths of the $(^1D_2)$ $10p$ $[2]_{3/2}$ and $7f$ $[2]_{3/2}$ resonances have been determined as 8(1) cm^{-1} and 7(1) cm^{-1}, respectively.

In Table I we present the level assignments, energies, and effective quantum numbers of all the observed transitions attached to the $4d^95s(^{1,3}D)7p$ and $4f$ configurations. In the following section we present the details of the series attached to each parent ionic level due to the $4d$-subshel excitation in silver.

A. $4d^95s(^3D_3)$ np, nf series

The series limit built on the $4d^95s(^3D_3)$ parent ionic level lies at 100 270.64 cm^{-1}, and the corresponding Rydberg series is $4d^95s(^3D_3)$ np $[2]_{3/2}$. The leading member of this series shows a broad autoionizing line shape. The identification of the higher members of the series was made based on analysis of quantum defects and line profiles (see Fig. 3). The series has been observed for $n=7-34$, which shows a considerably improved quality of the spectrum compared with the earlier data of Cantu *et al.* [5] who reported this series up to $n=24$. The leading members of the $4d^95s$ $(^3D_3)$

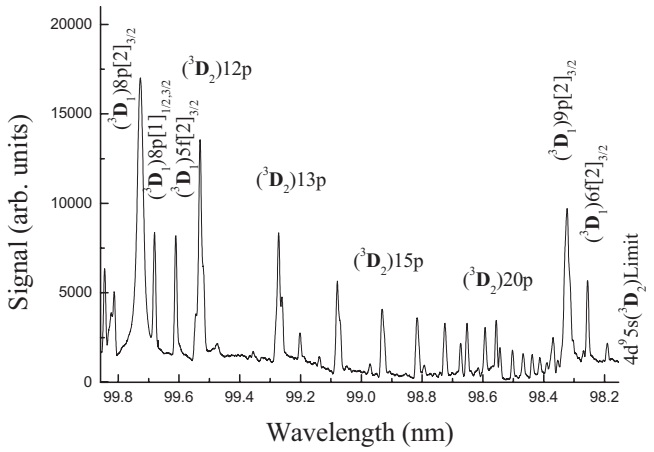

FIG. 8. Densitometer trace of the absorption spectrogram of silver in the 99.9–98.1-nm region showing the $4d^9\ 5s\ (^3D_2)\ np$ Rydberg series ($12 \leqslant n \leqslant$ limit). The two members of the series built on the $4d^9\ 5s\ (^3D_2)$ limit lying at both the ends of the spectra are dominating in this region.

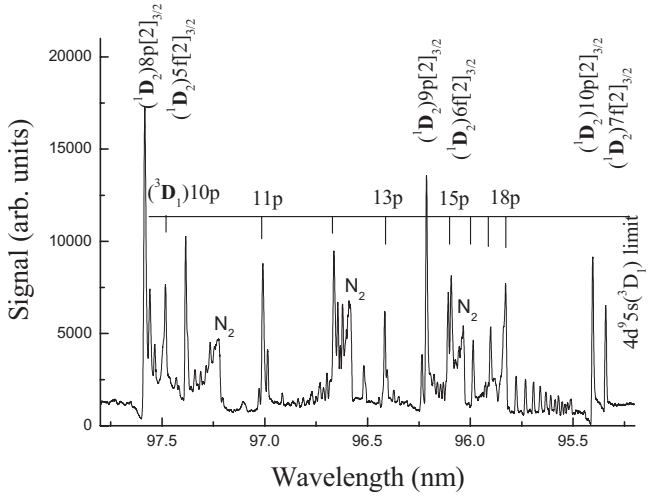

FIG. 9. Densitometer trace of the absorption spectrogram of silver in the 97.2–95.4-nm region showing the $4d^9\ 5s\ (^3D_1)\ np$ Rydberg series ($10 \leqslant n \leqslant$ limit). In addition to all the identified lines in this region, there are a few rovibrationic bands of nitrogen molecule which appear as impurity.

nf series ($n=4$ and 5) possess three lines that correspond to the $[0]_{1/2}$, $[1]_{1/2,3/2}$, and $[2]_{3/2}$ K components, respectively. The $[0]_{1/2}$ line is much weaker than the $[1]_{1/2,3/2}$ and $[2]_{3/2}$ lines. These lines merge into a single line after $n=7$, and the higher member of the nf series after $n=12$ could not be detected as the intensities of the lines decrease very sharply. Cantu *et al.* [5] reported only two nf series attached to this limit. We have extended these series and observed all their expected K components.

B. $4d^9 5s(^3D_2)\ np$, nf series

The $4d^9 5s\ (^3D_2)$ series limit is at 101 847.56 cm^{-1}, and its attached Rydberg series are $4d^9 5s\ (^3D_2)np\ [1]_{1/2,3/2}$, $[2]_{3/2}$. The lower member of this series starts as a group of three lines around 106.0–105.5 nm (see Fig. 1). The first line $7p\ [2]_{3/2}$ is well separated from the two overlapping $7p\ [1]_{3/2}$ and $7p\ [2]_{3/2}$ lines. The K components have been resolved up to $n=10$; afterwards, a single series is extended up to $n=37$. In Fig. 8 we reproduce the spectrum covering the wavelength region between 99.9 and 98.20 nm showing the higher Rydberg states close to the series limit. At the lower energy side of the spectrum, the $(^3D_1)8p\ [2]_{3/2}$, $[1]_{1/2,3/2}$ and $(^3D_1)5f[2]_{3/2}$ lines and at the higher-energy side, adjacent to the series limit, the $(^3D_1)9p\ [2]_{3/2}$ and $(^3D_1)6f[2]_{3/2}$ lines are evident which also inhibit the extension of these series close to the series limit. The $4d^9 5s\ (^3D_2)nf$ series have also been observed. The leading member show two K components, $4f\ [2]_{3/2}$ at 105.415 nm and $4f\ [1]_{1/2,3/2}$ at 105.397 nm as reproduced in Fig. 1. These lines are very sharp and weak as compared to the p series. The two K components are resolved for $n=4-6$; thereafter, single lines are observed up to $n=10$. The observed level structure also confirms the choice of j_cK coupling for the level assignments. Cantu *et al.* [5] also reported two nf series to this limit, one series up to $n=8$ and the other up to $n=11$. We agree with his assignments for one of the nf series, but the assignment of the other series needs to be revised based on the quantum defect analysis.

C. $4d^9 5s(^3D_1)\ np$, nf series

The $4d^9 5s(^3D_1)$ series limit lies at 104 845.26 cm^{-1}, and the Rydberg series built on this limit are $4d^9 5s\ (^3D_1)\ np\ [0]_{1/2}$, $[2]_{3/2}$, and $[1]_{1/2,3/2}$. The lower members of the series ($n=7$) are reproduced in Fig. 2. In Fig. 9 we show the higher members of the series covering the energy region between 97.75 and 95.25 nm. This part of the spectrum also contains a few molecular nitrogen absorption bands that distort the base line. At the lower-energy side of the spectrum, the $(^1D_2)8p\ [2]_{3/2}$ and $(^1D_2)5f[2]_{3/2}$ lines are apparent, whereas at the higher-energy side, neighboring the series limit, the $(^1D_2)10p\ [2]_{3/2}$ and $(^1D_2)7f[2]_{3/2}$ lines are located. For $n=8-11$, only three components have been observed and the series has been extended up to $n=34$. There is only one nf series attached to this limit, assigned as $4d^9 5s\ (^3D_1)\ nf\ [2]_{3/2}$. This series is weak and sharp in appearance and has been observed up to $n=12$ as the higher members are too weak to be detected.

D. $4d^9 5s\ (^1D_2)\ np$, nf series

The Rydberg series built on the $4d^9 5s(^1D_2)$ limit at 107 152.26 cm^{-1} are represented as $4d^9 5s(^1D_2)\ np\ [1]_{1/2,3/2}$ and $[2]_{3/2}$. The leading member of the series $(^1D_2)\ 7p\ [2]_{3/2}$ is located at 100.33 nm (see Fig. 3). This line does not show any broadening due to autoionization; its width 8(1) cm^{-1} is much smaller than the analogous members of the series built on the triplet ionic level. The next member of this series $(^1D_2)8p$ is observed around 97.6 nm. Interestingly, this line lies above the $4d^9 5s\ (^3D_2)$ limit and its line profile is clearly asymmetric with a minimum in the cross section at the lower-energy side (see Fig. 9). It seems that the levels built on the singlet parent ion level autoionize in to the $4d^9 5s\ (^3D_2)\ \varepsilon\ell$ continuum in contrast to the autoionization of the levels built on the triplet parent ion level which decay into the $3d^{10}\varepsilon\ell$ continuum. The $(^1D_2)10p$ and $(^1D_2)7f$ lines are

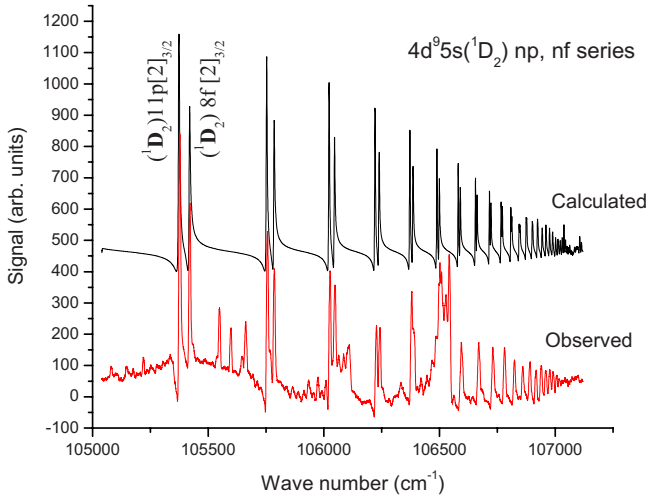

FIG. 10. (Color online) The observed and simulated Rydberg series of autoionizing resonances ($11 \leqslant n \leqslant$ limit) attached to the line $4d^9\ 5s\ (^1D_2)$ limit. The MQDT parameters are listed in the text.

well isolated and lie above the $4d^9 5s\ (^3D_1)$ limit. In Fig. 10 we reproduce the spectrum covering the region between 10 5000 and 107 025 cm^{-1} showing the higher members of the series along with the simulated spectra using the MQDT parameters determined from the $(^1D_2)10p$ and $(^1D_2)7f$ lines (see Fig. 7). The series has been observed up to $n=37$. The additional weak lines in between the Rydberg series are the rotational lines of molecular hydrogen [20,21] that have been used as wavelength standards to calculate the energies of the silver lines. The possible nf excited levels attached to this limit are $4d^9 5s(^1D_2)\ nf\ [1]_{1/2,3/2}$ and $[2]_{3/2}$. All the expected K components have not been observed for these levels. The $n=4$ leading member lies at 99.888 nm (see Fig. 3), and the series has been extended up to $n=17$. This series is reported in the present work.

In conclusion, the study of the $4d$-subshell excitation spectrum of silver conducted at a much higher dispersion and resolution reveals more detailed structure. A number of new series have been identified and the level assignments are made in the jK-coupling scheme based on quantum defects and line shapes analysis. As a result of the highly resolved spectra, some of the level assignments are revised. A full multiplicity of the K and J components of levels built on the triplet ionic levels $4d^9 5s\ (^3D_{3,2,1})$ has been observed, whereas only the K components have been observed for the levels attached to the singlet ionic level $4d^9 5s\ (^1D_2)$. An interesting observation is that the leading members of the np series attached to the triplet ionic levels $4d^9 5s\ (^3D_{3,2,1})$ are broad and symmetric, whereas the leading members of the np and nf series attached to the singlet ionic level $4d^9 5s\ (^1D_2)$ are sharp. The higher members that lie above the $4d^9 5s\ (^3D_2)$ limit possess asymmetric line profiles. A theoretical treatment of this problem might shed some more light on the configuration interactions of the levels built on the singlet and triplet ionic levels.

ACKNOWLEDGMENTS

I am grateful to the Alexander von Humboldt Stiftung for the financial assistance to visit the Bonn University, Germany where the experimental work was conducted. I am thankful to Professor J. Hormes for providing all the necessary experimental facilities and support during my stay in Bonn.

[1] K. Tegeder and R. Lincke, Z. Phys. **247**, 51 (1971).
[2] H. U. Johannsen and R. Lincke, Z. Phys. A **272**, 147 (1975).
[3] J. P. Connerade, M. A. Baig, M. W. D. Mansfield, and E. Radke, Proc. R. Soc. London, Ser. A **361**, 379 (1978).
[4] J. P. Connerade and M. A. Baig, Proc. R. Soc. London, Ser. A **365**, 253 (1979).
[5] A. M. Cantù, E. Jannitti, M. Mazzoni, M. Pettini, and G. Tondello, Phys. Scr. **19**, 283 (1979).
[6] G. K. James, K. J. Ross, and M. Wilson, J. Phys. B **16**, 4237 (1983).
[7] M. Müller, M. Schmidt, and P. Zimmermann, Europhys. Lett. **2**, 359 (1986).
[8] S. Baier, M. Martins, B. R. Müller, M. Schulze, and P. Zimmermann, J. Phys. B **23**, 3095 (1990).
[9] M. A. Baig, A. Rashid, M. Hanif, W. Dussa, I. Ahmad, and J. Hormes, Phys. Rev. A **45**, 2108 (1992).
[10] H. P. Loock, L. Beaty, and B. Simard, Phys. Rev. A **59**, 873 (1999).
[11] T. Badr, S. Guerandel, M. D. Plimmer, P. Juncar, and M. E. Himbert, Eur. Phys. J. D **14**, 39 (2001).
[12] J. C. Pickering and V. Zilio, Eur. Phys. J. D **13**, 181 (2001).
[13] K. Sommer, M. A. Baig, and J. Hormes, Z. Phys. D: At., Mol. Clusters **4**, 313 (1987).
[14] M. A. Baig, J. Phys. B **21**, L365 (1988).
[15] M. A. Baig, S. Ahmed, M. Akram, J. P. Connerade, and J. Hormes, J. Phys. B **25**, 1719 (1992).
[16] M. A. Baig, S. Ahmed, U. Griesmann, J. P. Connerade, S. A. Bhatti, and N. Ahmad, J. Phys. B **25**, 321 (1992).
[17] M. A. Baig, M. Akram, S. A. Bhatti, K. Sommer, and J. Hormes, J. Phys. B **27**, 1693 (1994).
[18] M. A. Baig, M. Hanif, S. A. Bhatti, and J. Hormes, J. Phys. B **30**, 5381 (1997).
[19] M. A. Baig, Eur. Phys. J. D **46**, 437 (2008).
[20] P. G. Wilkinson, Can. J. Phys. **46**, 225 (1968).
[21] M. A. Baig and J. P. Connerade, J. Phys. B **18**, L809 (1985).
[22] K. Yoshino and Y. Tanaka, J. Opt. Soc. Am. **69**, 159 (1979).
[23] C. Brown and M. L. Ginter, J. Opt. Soc. Am. **67**, 1323 (1977).
[24] T. Ishikawa, Jpn. J. Appl. Phys., Part 1 **33**, 2056 (1994).
[25] C. E. Moore, *Atomic Energy Levels, Natl. Bur. Stand (U.S.)*, Circular No. 467 (UPO, Washington, D.C., 1971). W. C. Martin and J. Sugar, J. Opt. Soc. Am. **59**, 1266 (1969).
[26] G. Racah, Phys. Rev. **61**, 537 (1942).

[27] R. D. Cowan, *Theory of Atomic Structure and Spectra* (University of California Press, Berkeley, 1981).
[28] U. Heinzmann, A. Wolke, and J. Kessler, J. Phys. B **13**, 3149 (1980).
[29] W. C. Cooke and C. L. Cromer, Phys. Rev. A **32**, 2725 (1985).
[30] A. Giusti-Suzor and U. Fano, J. Phys. B **17**, 215 (1984).
[31] K. Ueda, Phys. Rev. A **35**, 2484 (1987).
[32] T. F. Gallagher, *Rydberg Atoms* (Cambridge University Press, Cambridge, England, 1994).
[33] M. A. Baig and S. A. Bhatti, Phys. Rev. A **50**, 2750 (1994).